Journal of Nuclear Materials 389 (2009) 108–114

Contents lists available at ScienceDirect

Journal of Nuclear Materials

journal homepage: www.elsevier.com/locate/jnucmat

Electrochemical transient techniques for study of the electrochemistry and thermodynamics of nuclear materials in molten salts

S.A. Kuznetsov [a,*], M. Gaune-Escard [b]

[a] Institute of Chemistry, Kola Science Centre RAS, 14 Fersman Str., 184209 Apatity, Murmansk Region, Russia
[b] Ecole Polytechnique, Mecanique Energetique, Technopole de Chateau Gombert, 5 Rue Enrico Fermi, 13453 Marseille cedex 13, France

A B S T R A C T

Advantages and disadvantages of electrochemical transient techniques and potentiometry for the determination of formal standard potentials were discussed. It was shown that long potentiometric measurements inevitability led to strong interaction between oxide materials and melts involving actinide or lanthanide compounds. Reactions of disproportionation were observed in melts containing lower oxidation states due to the appearance of oxide ions from oxide materials, because actinides and lanthanides have a great affinity to oxygen. Only at the final stage of each experimental set, was the reference electrode immersed in the melt for a short time for the determination by electrochemical transient techniques and the melt being no longer used after these measurements. It was shown that electrochemical transient techniques in contradiction to potentiometry can be used for the determination of formal standard potentials for irreversible process and redox process accompanied by reaction of disproportionation.

1. Introduction

The pyrometallurgical process is now considered as one of the most promising options in an innovative nuclear fuel cycle [1]. The lanthanide (Ln) and actinide (An) elements present in spent fuel from fast nuclear reactors can be converted into molten salts by anodic dissolution [1]. The actinides (An) are selectively deposited at the cathode due to the differences among the redox potentials of the elements while fission products remain in the anode and in the electrolyte [2,3]. Due to their similar chemical properties the lanthanide elements are the most difficult fission products to separate from actinides. Until now, the various elements present in nuclear wastes are separated by hydrometallurgical processes. Accordingly, many investigations focus at the present time on alternative technologies based on pyrochemical processes for a more compact fuel cycle, allowing the reduction of all wastes. In such techniques, molten alkali halide salt baths are widely used.

Electrochemical transient techniques (ETT) is a powerful method for studying kinetics especially for the highly radioactive isotopes of Am and Cm, because the experiment should be carried out in limited time. In these pyrochemical processes, actinide and lanthanide chlorides are usually diluted in a molten salt medium. In this case, as we already showed [4,5], the electrochemical transient techniques is also an effective method for the determination of thermodynamic properties.

Nevertheless, before publication [4] there was a certain discussion about the correctness of non-stationary electrochemical methods for thermodynamic determinations in molten salts. Up to now, a certain opinion exists [6] that ETT can be used for rough marks, for example, of formal standard potentials of lanthanides, actinides in melts, and only the EMF method or potentiometry provide reliable data.

The aim of this study to describe our approach and advantages of electrochemical transient techniques in comparison with the EMF method and potentiometry for determining the Ln and An thermodynamic properties in molten salts.

2. Experimental

2.1. Chemicals

Synthesis of lanthanide chlorides was described in detail earlier [7–9]. Tetrachloride of uranium was synthesized from U_3O_8 (Merck) by hydrogen reduction to UO_2 and then by chlorination with CCl_4 vapors [10]. Trichloride of uranium was prepared by the oxidation of U with $CdCl_2$ in LiCl–KCl melt at 773 K [11]. Polarographic-grade alkali chlorides (NaCl, KCl, CsCl and NaF) were purchased from Prolabo (99.5 wt% min.) and they were recrystallized twice in a platinum crucible. LiCl–KCl eutectic and $CdCl_2$ were

* Corresponding author. Tel.: +7 815 55 797 30; fax: +7 815 55 616 58.
E-mail address: kuznet@chemy.kolasc.net.ru (S.A. Kuznetsov).

0022-3115/$ - see front matter © 2009 Elsevier B.V. All rights reserved.
doi:10.1016/j.jnucmat.2009.01.015

obtained from the Anderson Physics Laboratory. Li_2O (Merck, 98 wt%) was used with no additional purification.

Due to the highly hygroscopic character of Ln and An compounds, they were stored in sealed glass ampoules under vacuum. All further handling of Ln and An chlorides and filling of experimental cells were performed in a controlled and purified argon atmosphere in a glove-box (water content less than 2 ppm.). The total concentration of lanthanides and actinides was determined by inductively coupled plasma atomic spectroscopy (ICP-AES).

2.2. Procedures and electrochemical cell

Chlorides of alkali metals were placed in an ampoule made of glassy carbon (SU-2000 type) and were transferred to a hermetically sealed stainless steel retort. The latter was evacuated to a residual pressure of $5 \cdot 10^{-3}$ Torr, first at room temperature and then at higher temperatures (473, 673 and 873 K). The retort was then filled with high purity argon and the electrolyte was melted. The experiments were performed under argon (U-grade: <3 ppm H_2O and 2 ppm O_2) atmosphere. The cell was heated using a programmable furnace and temperatures were measured using Pt–PtRh (10%) thermocouple.

Investigations were performed employing several experimental methods, linear sweep voltammetry (LSV), cyclic voltammetry (CV), chronopotentiometry (CP), chronoamperometry (CA) and electrochemical impedance spectroscopy (EIS) using a VoltaLab-40 potentiostat with packaged software 'VoltaMaster 4' version 6 and a potentiostat/galvanostat PAR EG&G Model 273 controlled by the PAR EG&G M270/250 4.40 software package. Experiments were carried out in a temperature range 723–1123 K. The electrochemical curves were recorded on tungsten (1 mm diameter) and glassy carbon electrodes (0.8–2.0 mm diameter) with respect to a glassy carbon plate as a quasi-reference electrode. The glassy carbon ampoule served as the counter electrode. The GC quasi-reference electrode monitored the redox potential of the melt, which remained constant, if the composition of the melt unchanged. While the potential of this quasi-reference electrode does not constitute a thermodynamic reference, its use was preferred in order to avoid any contact between the melt and oxygen-containing material as used in classical reference electrodes. A Ag/NaCl–KCl–AgCl (2 wt%) reference electrode was used in order to obtain more reliable potential values. At the final stage of each experimental set, this reference electrode was immersed in the melt for a short time for determination of the potential peaks, the melt being no longer used after these measurements. The potentials from silver–silver chloride reference electrode were converted to a Cl^-/Cl_2 reference electrode [12].

2.3. Electrochemical control of impurities

The main impurities in lanthanide and actinide chlorides are oxide, hydroxide and water. Cyclic voltammetry was used to determine the quality of synthesized Ln and An compounds after their addition to the melt. The cyclic voltammogram at glassy carbon electrode in $CsCl–YbCl_3$ melt is presented in Fig. 1. The peaks R_1 and Ox_1 correspond to the redox process $Yb(III) + e^- \leftrightarrow Yb(II)$, waves R_2, Ox_2 are responsible for discharge of alkali metals cations and dissolution of alkali metals. The small wave Ox_3 is connected with electroreduction of oxide and hydroxide ions and Ox_4 corresponds to oxidation of chloride ions. The wave Ox_3 was not visible in CsCl melt and the appearance of this wave was clearly demonstrated the certain contamination of impurities in $YbCl_3$. The current density of the process Ox_3 should be much smaller compared to the ytterbium redox reaction. The significant wave Ox_3 indicates conclusively of the necessity of additional purification.

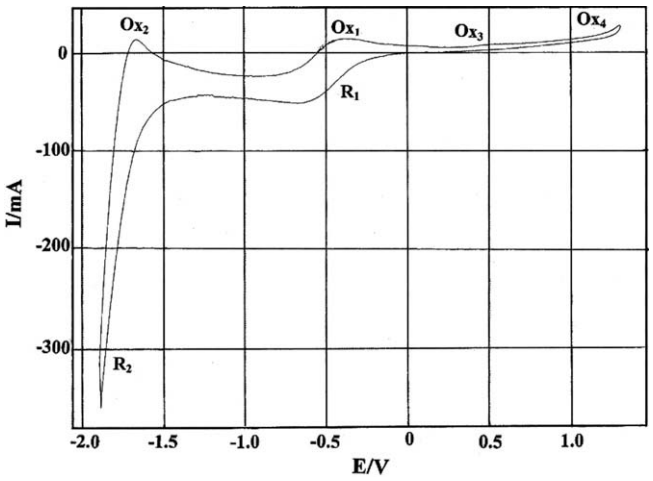

Fig. 1. Cyclic voltammogram at a glassy carbon electrode in $CsCl–YbCl_3$ melt. Area: 0.659 cm^2. Sweep rate: 0.1 V s^{-1}. Temperature: 973 K. Concentration of $YbCl_3$: $6.21 \cdot 10^{-5}$ mol cm^{-3}. Reference electrode: silver–silver chloride.

3. Results and discussion

3.1. Interaction of oxide materials with LiCl-KCl-UCl_4 and LiCl-KCl-UCl_3 melts

Transformation of voltammetric curves after the addition of oxide ions (Li_2O) to the melt $LiCl–KCl–UCl_4$ is shown in Fig. 2. After Li_2O introduction to the uranium-containing melt the heights of

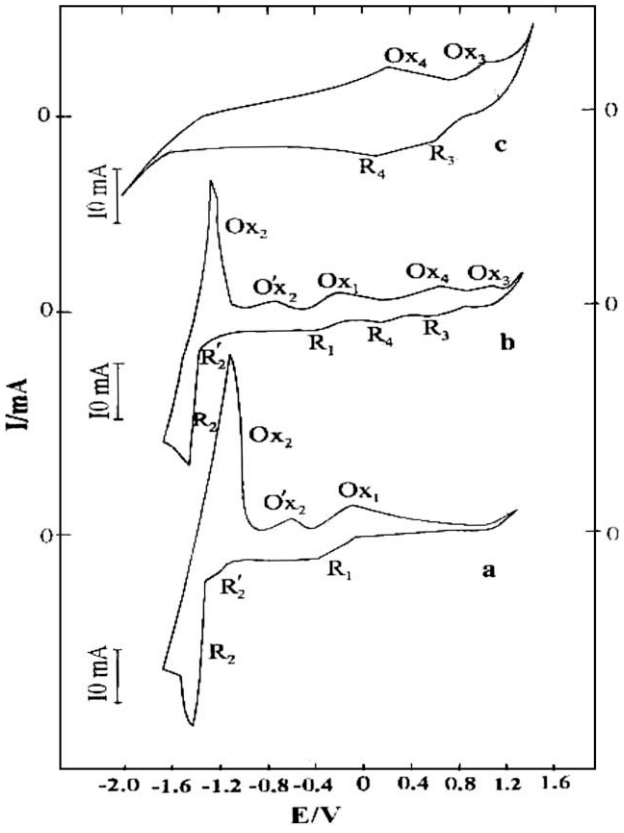

Fig. 2. Cyclic voltammetric curves at a tungsten electrode in $LiCl–KCl–UCl_4–Li_2O$ melt at different ratios of $O^{2-}/U(IV)$. (a) 0; (b) 0.23; (c) 1.4. Area: 0.407 cm^2. Sweep rate: 0.5 V s^{-1}. Initial concentration of UCl_4: $4.61 \cdot 10^{-5}$ mol cm^{-3}. Reference electrode: silver–silver chloride.

the waves (R_1, R_2), corresponding to the electroreduction of uranium chloride complexes [13–15]:

$$U(IV) + e^- \rightarrow U(III), \quad (1)$$

$$U(III) + 3e^- \rightarrow U, \quad (2)$$

decreased and two new waves (R_3, R_4) appeared at more positive potentials (Fig. 2(b)). Finally, at the ratio $O^{2-}/U(IV) = 1.3–1.5$ only these two waves (R_3, R_4) remained on the voltammetric curve (Fig. 2(c)). It is possible to suggest that the following chemical reaction proceeds in the melt:

$$3UCl_6^{2-} + 4O^{2-} \leftrightarrow 2UO_2^{2+} + U + 18Cl^-. \quad (3)$$

Titration by oxide ions of LiCl–KCl–UCl_3 melt results in the next reaction:

$$2UCl_6^{3-} + 2O^{2-} \leftrightarrow UO_2^{2+} + U + 12Cl^-. \quad (4)$$

After the interaction of oxide ions with LiCl–KCl melt containing UCl_4 or UCl_3, the color of the melt was yellow, which indicated the formation of U(VI) complexes. Actually, the addition of UO_2Cl_2 to the melts led to increasing the peak currents of waves R_3 and R_4. Thus, waves 3 and 4 observed on the voltammetric curves (Fig. 2) correspond to electroreduction of the uranyl-chloride complexes [16]:

$$UO_2^{2+} + e^- \rightarrow UO_2^+, \quad (5)$$

$$UO_2^+ + e^- \rightarrow UO_2. \quad (6)$$

As was shown in [17] analogous transformation of voltammograms was observed also during a long contact (5–7 h) of oxide material (alumina, Pyrex) with LiCl–KCl–UCl_4 and LiCl–KCl–UCl_3 melts, because the same reactions of disproportionation (3) and (4) occur due to a change of the anionic composition of the melt and the appearance of oxide anions in the melt resulting from oxide materials corrosion. Additionally, peaks corresponding to the discharge of boron and silicon species formed due to the corrosion of Pyrex in the LiCl–KCl–UCl_4 melt (silicon and boron are the main components of Pyrex) were identified [18]. Especially strong interaction of alumina and Pyrex was observed in LiCl–KCl–UCl_3 melt, which was accompanied by the formation of a conductive dark film on the surface of oxide materials. Mostly the conductive film is the product of uranium interaction with oxide materials.

3.2. Interaction of oxide materials with lanthanide chlorides

In studies [6,19–23] concerning the electrochemistry of lanthanide chlorides oxide materials such as quartz, glass and alumina were used in construction of electrochemical cell. Even at temperature 723 K we observed corrosion of oxide materials in LiCl–KCl melt containing $LnCl_3$ and $LnCl_2$. In the course of experiments the lanthanide concentration decreased continuously, but in distinction to electrochemical behavior of uranium on the voltammograms, new waves corresponding to lanthanide oxychloride complexes, did not appear. The wave Ox_3 (Fig. 1), which is connected with electrooxidation of oxide ions, did not increase too. Nevertheless, the formation of a conductive film on the surface of oxide materials after contact with melts containing Ln(III) and Ln(II) is evidence of a strong interaction. This interaction can be described by the next reaction:

$$3LnCl_4^{2-} + 2O^{2-} \leftrightarrow 2LnOCl + Ln + 10Cl^-. \quad (7)$$

Even the small concentration of oxide in the construction of the electrochemical cell caused the reaction of disproportionation (7). The formation of conductive NdB_6 film was found on the surface of sintered boron nitride (0.2–0.4 wt% of oxygen) after its interaction with the $NdCl_3$ (50 mol%)–$NdCl_2$ (50 mol%) at temperature 1133 K (Fig. 3). At the same time, the surface of pyrolytic boron nitride (0.003 wt% of oxygen) had not changes after the same test. The reason for such a different behavior is boric oxide impurity in sintered boron nitride which led to the disproportionation:

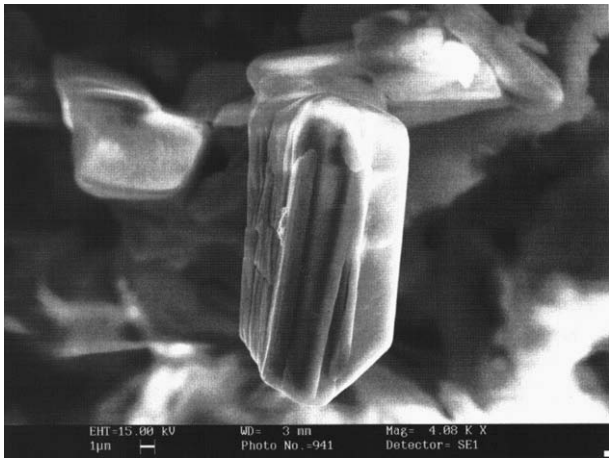

Fig. 3. Micrograph of NdB_6, obtained on boron nitride after 7 h on contact with $NdCl_3$ (50 mol%)–$NdCl_2$ (50 mol%) melt. Temperature: 1133 K.

$$3NdCl_4^{2-} + 2O^{2-} \leftrightarrow 2NdOCl + Nd + 10Cl^-, \quad (8)$$

with the following interaction of neodymium with boron nitride.

3.3. Advantages and disadvantages of electrochemical transient techniques and potentiometry method for the determination of formal standard redox potentials $E^*_{Ln(III)/Ln(II)}$

3.3.1. Reversible processes

It was shown in our studies [5,12,24–26] that in NaCl–KCl, KCl and CsCl melts redox process:

$$Ln(III) + e^- \leftrightarrow Ln(II), \quad (9)$$

(where Ln–Sm, Eu, Yb) is reversible up to the scan rate 0.1 V s^{-1},

The cyclic voltammetric curves in CsCl–$YbCl_3$ melt obtained at the glassy carbon electrode are presented in Fig. 4. It was found that the peak current is directly proportional to the square root of the polarization rate, while the peak potential does not depend on the polarization rate up to $v = 0.1$ V s^{-1}. The peak current of the electroreduction process is linearly dependent on the $LnCl_3$ concentration, while the peak potential does not depend on the concentration of lanthanide trichloride in the melt. On the basis of the obtained diagnostic criteria [27] it is possible to conclude that up to polarization rate of 0.1 V s^{-1} the electrode process (9) is controlled by the rate of mass transfer.

According to the theory of linear sweep and steady state voltammetry the following relations are valid for the reversible electrochemical reduction (9) between the cathodic and anodic peak potentials and half-wave potential [28]:

$$E_p^C = E_{1/2} - 1.11(RT/F), \quad (10)$$

$$E_p^A = E_{1/2} + 1.11(RT/F), \quad (11)$$

$$(E_p^C + E_p^A)/2 = E_{1/2}, \quad (12)$$

where

$$E_{1/2} = E^0_{Ln(III)/Ln(II)} + (RT/F) \cdot \ln(D_{red}/D_{ox})^{1/2} + (RT/F) \cdot \ln(\gamma_{ox}/\gamma_{red}). \quad (13)$$

In the concentration range of ions with mole fraction less than $(3–5) \cdot 10^{-2}$ the coefficients of activity in the molten salts remain constant and leads up to the values of the formal standard potentials [29]:

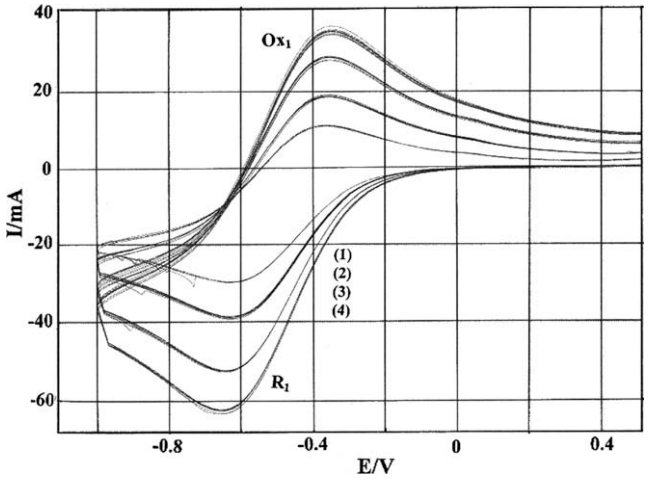

Fig. 4. Cyclic voltammetric curves at a glassy carbon electrode for the redox process $Yb(III) + e^- \leftrightarrow Yb$ in CsCl–$YbCl_3$. Sweep rates (1): 0.05; (2): 0.1; (3): 0.2; (4): 0.3 V s^{-1}. Temperature: 973 K. Concentration of $YbCl_3$: $6.03 \cdot 10^{-5}$ mol cm^{-3}. Reference electrode: silver–silver chloride.

$$E^*_{Ln(III)/Ln(II)} = E^0_{Ln(III)/Ln(II)} + (RT/F) \cdot \ln(\gamma_{ox}/\gamma_{red}). \quad (14)$$

Thus the formal standard redox potentials of $E^*_{Eu(III)/Eu(II)}$ can be calculated from the following equations:

$$E^*_{Ln(III)/Ln(II)} = E_{1/2} + (RT/F) \cdot \ln(D_{ox}/D_{red})^{1/2}, \quad (15)$$

$$E^*_{Ln(III)/Ln(II)} = E_{\tau/4} + (RT/F) \cdot \ln(D_{ox}/D_{red})^{1/2}, \quad (16)$$

$$E^*_{Ln(III)/Ln(II)} = E^C_p + 1.11(RT/F) + (RT/F) \cdot \ln(D_{ox}/D_{red})^{1/2}, \quad (17)$$

$$E^*_{Ln(III)/Ln(II)} = E^A_p + 1.11(RT/F) + (RT/F) \cdot \ln(D_{ox}/D_{red})^{1/2}, \quad (18)$$

$$E^*_{Ln(III)/Ln(II)} = (E^C_p + E^A_p)/2 + (RT/F) \cdot \ln(D_{ox}/D_{red})^{1/2}, \quad (19)$$

where τ is the transition time.

For the calculation of $E^*_{Ln(III)/Ln(II)}$ we used mostly Eqs. (17)–(19) because the values E^C_p and E^A_p are more reproducible compared to the values for $E_{1/2}$ and $E_{\tau/4}$.

Thus using the values of potential peaks of the redox process and the diffusion coefficients of Ln(III) and Ln(II) [26] it was found that the formal standard redox potentials are described by the following empirical dependencies relative to the Cl^-/Cl_2 reference electrode [26]:

Samarium:

$$E^*_{Sm(III)/Sm(II)}/V = -(2.671 \pm 0.009) + (6.7 \pm 0.2) \cdot 10^{-4} T/K \quad (NaCl—KCl), \quad (20)$$

$$E^*_{Sm(III)/Sm(II)}/V = -(2.789 \pm 0.006) + (7.3 \pm 0.2) \cdot 10^{-4} T/K \quad (KCl), \quad (21)$$

$$E^*_{Sm(III)/Sm(II)}/V = -(2.990 \pm 0.005) + (8.4 \pm 0.2) \cdot 10^{-4} T/K \quad (CsCl). \quad (22)$$

Europium:

$$E^*_{Eu(III)/Eu(II)}/V = -(0.971 \pm 0.006) + (1.9 \pm 0.2) \cdot 10^{-4} T/K \quad (NaCl—KCl), \quad (23)$$

$$E^*_{Eu(III)/Eu(II)}/V = -(1.008 \pm 0.008) + (2.1 \pm 0.3) \cdot 10^{-4} T/K \quad (KCl), \quad (24)$$

$$E^*_{Eu(III)/Eu(II)}/V = -(1.418 \pm 0.005) + (4.2 \pm 0.2) \cdot 10^{-4} T/K \quad (CsCl). \quad (25)$$

Ytterbium:

$$E^*_{Yb(III)/Yb(II)}/V = -(1.990 \pm 0.007) + (3.2 \pm 0.2) \cdot 10^{-4} T/K \quad (NaCl-KCl), \quad (26)$$

$$E^*_{Yb(III)/Yb(II)}/V = -(2.145 \pm 0.007) + (4.0 \pm 0.2) \cdot 10^{-4} T/K \quad (KCl), \quad (27)$$

$$E^*_{Yb(III)/Yb(II)}/V = -(2.397 \pm 0.005) + (5.4 \pm 0.2) \cdot 10^{-4} T/K \quad (CsCl). \quad (28)$$

Analysis of Eqs. (20)–(28) showed that at the same temperature and in the same molten system the redox couple Sm(III)/Sm(II) has a more negative potential than that of for Eu(III)/Eu(II) and Yb(III)/Yb(II) redox couples. This is in accordance with studies [19,30]. Typical complexes of dilute solution lanthanide chlorides in alkali chloride melts are $LnCl_6^{3-}$ and $LnCl_4^{2-}$ [31]. Their relative stability increases with the increasing of cation radius and the formal standard redox potentials are shifted to the negative values. Our results are in an agreement with literature data [29] concerning the second coordination sphere influence on the formal standard redox potentials.

The formal standard redox potentials $E^*_{Sm(III)/Sm(II)}$ and $E^*_{Eu(III)/Eu(II)}$ were measured by direct potentiometry vs. a chlorine electrode [19]. There is a certain difference between our data and study [19]. In our opinion, this difference can be explained by some experimental disadvantages of this investigation, because oxide materials were used for crucible and the construction of reference electrode. Long potentiometric measurements, inevitability, as was shown in Section 3.2, led to the interaction of oxide materials with the melt which is described by the reaction (7). The occurrence of this reaction changes the ratio of Ln(III)/Ln(II) on the melt. To determine correctly the ratio of Ln(III)/Ln(II) is not too simple a task, because the mistake can be obtained from results of chemical analyses on the concentration of Ln(III) and Ln(II) in the electrolyte, especially due to the change of temperature from 1123 K to room temperature. Thus a disadvantage of potentiometry is a long contact of oxide material with the melt. Oxide material is used at least in the construction of the classical reference electrode and due to this the reaction (7) arises in the melt. At the same time, in ETT measurements and only at the final stage of each experimental set, the reference electrode was immersed in the melt for a short time for the determination of the potential peaks and the melt after these measurements was no longer used.

The disadvantage of some non-stationary methods, for instance, of cyclic voltammetry is the necessity of ohmic drop compensation for careful determination of peak potentials, but this is not a particular problem.

3.3.2. Irreversible and quasi-reversible process

The potentiometry method is unsuitable for the estimation of formal standard redox potentials for irreversible processes.

At the same time the formal standard redox potentials of $E^*_{Ln(III)/Ln(II)}$ for the irreversible process can be determined by means of the following equations [32]:

$$E^*_{Ln(III)/Ln(II)} = E_p + RT/\alpha n_\alpha F[0.78 - \ln k_s + \ln(\alpha n_\alpha F v D_{ox}/RT)^{1/2}]. \quad (29)$$

Thus for the calculation of $E^*_{Ln(III)/Ln(II)}$ it is necessary to obtain the voltammetric peak potential (E_p) and the kinetic parameters such as transfer α and diffusion coefficients (D_{ox}), and standard rate constants of charge transfer (k_s).

The cyclic voltammetric curves of the process:

$$Eu(III) + e^- \leftrightarrow Eu(II), \quad (30)$$

in the NaCl–KCl–$EuCl_3$ melt at the molar ratio F/Eu = 6 obtained at the glassy carbon electrode are presented in Fig. 5. At the polarization rate 0.2 V s^{-1}, process (30) is at least quasi-reversible, (i.e. the diffusion rate approached the rate of electron transfer) and the difference between anodic and cathodic peaks at this rate reached the value 0.601 V (Fig. 5).

Increasing the sweep rate from 0.3 to 2.0 V s^{-1} results in irreversible electroreduction because the peak current is directly proportional to $v^{1/2}$ (Fig. 6(a)), while the peak potentials shift to the cathodic direction with increasing of scan rate (Fig. 6(b)).

In the coordinates $E_P - \log v$ (Fig. 6(b)) the following slope was found at the temperature 1073 K:

$$K = 2.303\ RT/2\alpha n_\alpha F = 0.231\ V, \tag{31}$$

where α is the electrochemical transfer coefficient and n_α is the number of transferred electrons. So the product αn_α can be calculated by the expression:

$$\alpha n_\alpha = 2.303\ RT/2KF = 0.46. \tag{32}$$

This value, also at the same temperature 1073 K, is very close to those αn_α, which were found from the expressions described in [28,32]:

$$E_p - E_{p/2} = -1.857\ RT/\alpha n_\alpha F, \tag{33}$$

$$E_p^2 - E_p^1 = (RT/\alpha n_\alpha F)\cdot \ln(v^1/v^2). \tag{34}$$

The diffusion coefficients for the Eu(III) complexes were determined in the temperature interval 973–1123 K, at a polarization rate $v = 1.0$ V s^{-1} (at this rate the double layer charging current was virtually insignificant relative to the Faradaic current), using the Delahay equation for irreversible electrochemical processes [33]:

$$I_p^C = 0.496nFCAD^{1/2}(\alpha n_\alpha Fv/RT)^{1/2}, \tag{35}$$

where I_p^C is the peak cathodic current (A), A is the electrode area (cm^2), C is the bulk concentration of active species (mol cm^{-3}), D is the diffusion coefficient (cm^2 s^{-1}), v is the potential sweep rate (V s^{-1}) and n is the number of electrons involved in the reaction.

Equation of the Randles-Shevchik [33] was employed for calculating the diffusion coefficients of Eu(II) on the basis of the peak current determined for oxidation of Eu(II) to Eu(III). The temperature dependence of the logarithms of Eu(III) and Eu(II) diffusion coefficients can be expressed by the equations:

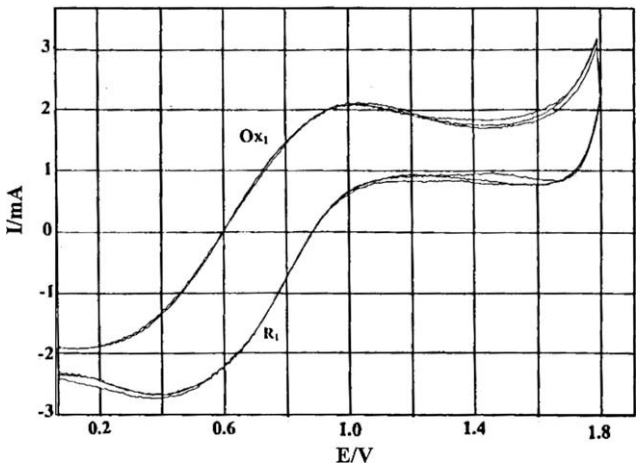

Fig. 5. Cyclic voltammetric curves at glassy carbon electrode in NaCl–KCl–$EuCl_3$–NaF melt. Area: 0.310 cm^2. Sweep rate: 0.2 V s^{-1}. Temperature: 973 K. Concentration of $EuCl_3$: $5.70 \cdot 10^{-5}$ mol cm^{-3}. Molar ratio F/Eu = 6. Quasi-reference electrode: glassy carbon.

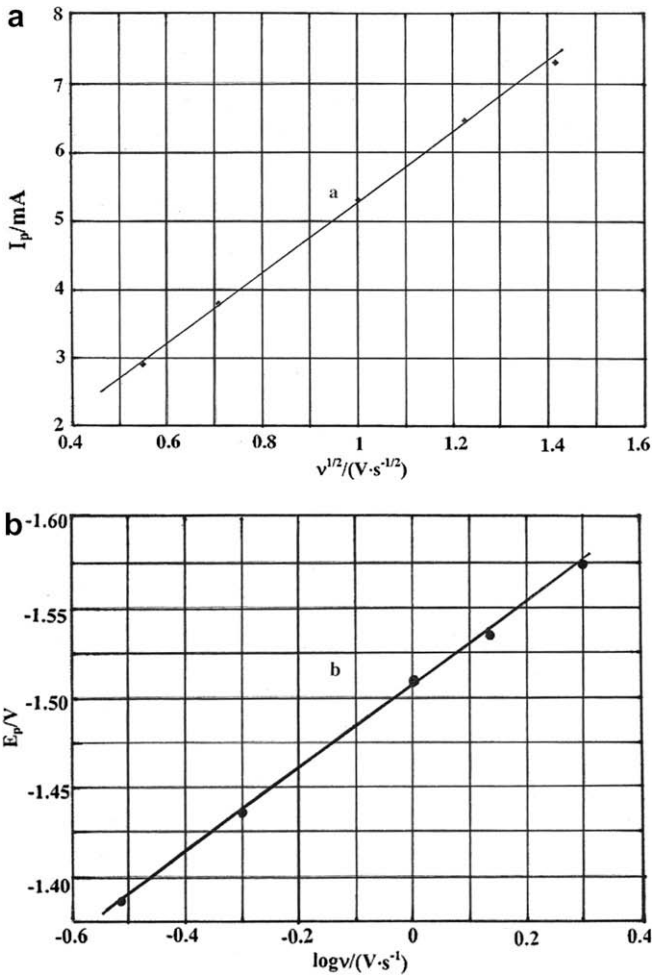

Fig. 6. The dependencies of peak currents (a) and of peak potentials of the redox process on the polarization rate. Area: 0.256 cm^2. Temperature: 1073 K. Concentration of Eu(III): $3.45 \cdot 10^{-5}$ mol cm^{-3}. Reference electrode: Cl^-/Cl_2.

$$\log D_{Eu(III)} = -2.22 - 2445/T \pm 0.03, \tag{36}$$

$$\log D_{Eu(II)} = -2.20 - 2365/T \pm 0.03. \tag{37}$$

The problem of determining standard rate constants of charge transfer on the basis of cyclic voltammetry was considered by Nicholson [34]. The standard rate constant of the electrode process is related to the function ψ as follows:

$$\psi = \frac{k_s(D_{ox}/D_{red})^{\alpha/2}}{\pi^{1/2}D_{ox}^{1/2}(nF/RT)^{1/2}v^{1/2}}. \tag{38}$$

Here ψ is a function related to the difference between the peak potentials E_p^A and E_p^C (mV), k_s is the standard rate constant of electrode process (cm s^{-1}), $\alpha = 0.5$ is the transfer coefficient. The dependencies $E_p^A - E_p^C$ on the function ψ reported in [34] at the temperature 298 K, must be recalculated for the present working temperature. The following equations were used [35]:

$$(\Delta E_p)_{298} = (\Delta E_p)_T 298/T, \tag{39}$$

$$\psi_T = \psi_{298}(T/298)^{1/2}, \tag{40}$$

and these values of the ψ_T function, used in conjunction with expression (38) made it possible to calculate the standard rate constants of charge transfer. The Eq. (38) is valid for quasi-reversible process so all results were obtained at the scan rate 0.2 V s^{-1}. The influence of the temperature on the standard rate constants of the electrode reaction (30) is presented in Table 1. The standard rate constants of charge transfer can be determined by EIS too.

Table 1
Influence of the temperature on the standard rate constants of charge transfer for the redox reaction Eu(III) + $e^- \leftrightarrow$ Eu(II) in an equimolar NaCl–KCl melt with molar ratio F/Eu = 6.

Temperature (K)	973	1023	1073
$(\Delta E_p)_T$ (V)	0.601	0.576	0.547
ψ_T	0.281	0.343	0.434
k_s (cm s^{-1})	$2.5 \cdot 10^{-3}$	$3.4 \cdot 10^{-3}$	$5.1 \cdot 10^{-3}$

The formal standard redox potential $E^*_{Eu(III)/Eu(II)}$ in the temperature range 973–1123 K were calculated using Eq. (29) and the temperature dependence $E^*_{Eu(III)/Eu(II)}$ is described by the following empirical relation:

$$E^*_{Eu(III)/Eu(II)} = -(1.664 \pm 0.008) + (4.6 \pm 0.2) \cdot 10^{-4} T/\mathrm{K}. \quad (41)$$

Some authors used Eqs. (15)–(19) for the quasi-reversible or even for irreversible processes that is not correct. In our opinion, the most relevant procedure for the determination $E^*_{Ln(III)/Ln(II)}$ in the case of quasi-reversible processes is to use polarization rates corresponding to the irreversibility of the process making it possible to use above describing approach.

3.4. Formal standard potentials $E^*_{Ln(III)/Ln}$ and $E^*_{An(III)/An}$

3.4.1. Reversible processes

The potentiometry has the same lack due to corrosion as for the estimation $E^*_{Ln(III)/Ln(II)}$, but it is necessary to note that the corrosion in melts containing only Ln(III) is smaller in comparison with molten systems containing Ln(III) and Ln(II). Interaction of oxide materials with melts involving actinide trichlorides is very strong (Section 3.1).

In the case of reversible process, the formal standard potentials for lanthanides and actinides can be calculated using LSV and equation [32]:

$$E^*_{Ln(III)/Ln} = E_p - (RT/nF)\ln N + 0.854\ RT/nF, \quad (42)$$

where N – concentration of Ln (III) in mole fraction.

The formal standard potentials of $E^*_{La(III)/La}$ in eutectic LiCl–KCl were determined [36] using the Eq. (42).

3.4.2. Irreversible and quasi-reversible process

The method of attack for the determination of formal standard potentials $E^*_{Ln(III)/Ln}$ and $E^*_{An(III)/An}$ is the same as discussed in Section 3.3.2. Only in this case due to the formation of metallic phase at the electrode, the method of Nicholson is not valid, because the difference between cathodic and anodic peaks depends on the quantity of metal deposited during the cathodic semi-cycle. The electrochemical impedance spectroscopy is suitable for the estimation of standard rate constants. Fig. 7 shows cyclic voltammetric curves at a tungsten electrode in LiCl–KCl–UCl_3 melt and a typical complex impedance diagram (Nyquist plot) is presented in Fig. 8. It is evident that the complex impedance diagram consists of two parts: one capacity loop on the higher frequency side is due to the kinetic control by an electrochemical charge transfer stage at the electrode–electrolyte interface and the straight line with the slope of about 45° on the lower frequency is attributed to diffusion of U(III) species. The following equation can be used for the charge transfer resistance (R_{CT}) at the rest potentials [37]:

$$R_{CT} = RT/nFi_0 = RT/n^2F^2k_sC^{1-\alpha}_{U(III)}, \quad (43)$$

where i_0 is the exchange current density. This expression allows us to calculate standard rate constants of charge transfer. As can be seen from the Fig. 8 the charge transfer resistance (R_{CT}) at temperature 723 K is equal to 0.32 Ω. The calculation showed that $k_s = 1.8 \cdot 10^{-4}$ cm s^{-1}.

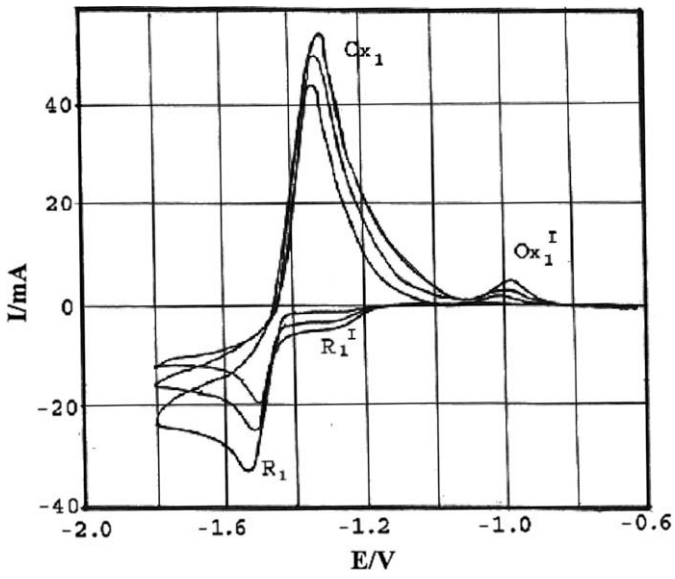

Fig. 7. Cyclic voltammetric curves at a tungsten electrode in LiCl–KCl–UCl_3 melt. Area: 0.322 cm^2. Sweep rates: 0.1; 0.2; 0.25 V s^{-1}. Temperature: 723 K. Concentration of UCl_3: $6.26 \cdot 10^{-5}$ mol cm^{-3}. Reference electrode: silver–silver chloride.

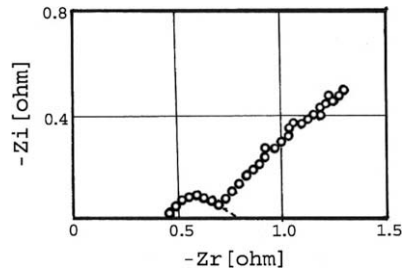

Fig. 8. Nyquist plot in LiCl–KCl–UCl_3 melt at rest potential −0.6 V vs. silver–silver chloride electrode. Area: 0.165 cm^2. Temperature: 723 K. Concentration of UCl_3: $5.68 \cdot 10^{-5}$ mol cm^{-3}. The frequency ranges 100 mHz ⩽ w ⩽ 100 kHz.

The formal standard potentials of $E^*_{U(III)/U}$ were determined by Eq. (29). Using the values of peak potentials at v = 0.5 V s^{-1} and obtained kinetic parameters ($D_{U(III)}$, k_s) the formal standard potentials were calculated (Table 2). From the data in Table 2 the following empirical equation for the formal standard potentials of $E^*_{U(III)/U}$ was obtained [36]:

$$E^*_{U(III)/U}/V = -(2.931 \pm 0.009) + (5.4 \pm 0.2) \cdot 10^{-4} T/\mathrm{K}. \quad (44)$$

3.5. Determination of formal standard redox potentials $E^*_{Ln(III)/Ln(II)}$ and $E^*_{An(III)/An(II)}$ for redox process accompanied by reaction disproportionation

This kind of process is typical for electroreduction of Nd(III), Am(III) and Cm(III) in molten salts. For example, the reduction process of Am(III) to Am(II) is complicated by the disproportionation reaction (DPP):

Table 2
Experimental and calculated data for determination of $E^*_{U(III)/U}$ in LiCl–KCl melt.

Temperature (K)	723	773	823
E_p (V)	−2.744	−2.722	−2.701
$D_{U(III)}$ (cm^2 s^{-1})	$1.02 \cdot 10^{-5}$	$1.45 \cdot 10^{-5}$	$1.97 \cdot 10^{-5}$
k_s (cm s^{-1})	$1.8 \cdot 10^{-4}$	$2.6 \cdot 10^{-4}$	$3.4 \cdot 10^{-4}$
$E^*_{U(III)/U}$	−2.541	−2.514	−2.487

$$Am(III) + e^- \rightarrow Am(II), \quad (45)$$

$$3Am(II) \leftrightarrow 2Am(III) + Am. \quad (46)$$

The potentiometry is unavailable in this case. The ignorance of the reaction DPP can lead to incorrect values of formal standard redox potentials, because occurring of reaction (46) influences on the value of peak potentials [32]. So such conditions should be found to prevent reaction (46). Usually the elimination of reaction (46) can be achieved by the application of high sweep rate which allows using the approach for reversible or irreversible processes.

4. Conclusions

Advantages and disadvantages of electrochemical transient techniques and potentiometry for the determination of formal standard potentials were discussed. It was shown that electrochemical transient techniques offer several advantages over potentiometry. The main convenience of electrochemical transient techniques is the possibility of formal standard potentials determination for irreversible process and redox process accompanied by reaction of disproportionation.

Acknowledgement

SAK wishes to thank the Ecole Polytechnique de Marseille for hospitality and support during this work.

References

[1] Y.I. Chang, Nucl. Technol. 88 (1989) 129.
[2] T. Koyama, M. Iizuka, Y. Shoji, et al., J. Nucl. Sci. Technol. 34 (1997) 384.
[3] A. Leseur, CEA Report No. 3793, 1969, 98p.
[4] S.A. Kuznetsov, E.G. Polyakov, P. T Stangrit, Dokl. Akad. Nauk USSR 273 (1983) 653.
[5] S. A Kuznetsov, L. Rycerz, M. Gaune-Escard, Z. Naturforsch. 56a (2001) 741.
[6] V.A. Khokhlov, A.V. Novoselova, E.V. Nikolaeva, O.Yu. Tkacheva, A.B. Salyulev, Rus. J. Electrochem. 43 (2007) 961.
[7] L. Rycerz, M. Gaune-Escard, High Temp. Mater. Process. 2 (1998) 483.
[8] L. Rycerz, M. Gaune-Escard, Z. Naturforsch. 57a (2002) 79.
[9] L. Rycerz, M. Gaune-Escard, Z. Naturforsch. 57a (2002) 215.
[10] H. Matsuura, Thesis, Tokyo Institute of Technology, Tokyo, 1997.
[11] D.S. Poa, Z. Tomczuk, R.K. Steunenberg, J. Electrochem. Soc. 135 (1988) 1161.
[12] S.A. Kuznetsov, M. Gaune-Escard, Electrochim. Acta 46 (2001) 1101.
[13] O. Shirai, T. Awai, Y. Suzuki, Y. Sakamura, H. Tanaka, J. Alloys Comp. 271–273 (1998) 685.
[14] B.P. Reddy, S. Vandarkuzhali, T. Subramanian, P. Venkatesh, Electrochim. Acta 49 (2004) 2471.
[15] K. Serrano, P. Taxil, J. Appl. Electrochem. 29 (1999) 497.
[16] J.C. Fondanaiche, T. Kikindai, Bull. Soc. Chim. France 875 (1966).
[17] S.A. Kuznetsov, H. Hayashi, K. Minato, M. Gaune-Escard, Electrochemistry 73 (2005) 630.
[18] S.A. Kuznetsov, H. Hayashi, K. Minato, M. Gaune-Escard, J. Electrochem. Soc. 152 (2005) C203.
[19] A. Novoselova, V. Shishkin, V. Khokhlov, Z. Naturforsch. 56a (2001) 754.
[20] Y. Castrillejo, M.R. Bermejo, E. Barrada, A.M. Martinez, Electrochim. Acta 51 (2006) 1941.
[21] M.R. Bermejo, F. De la Rosa, E. Barrado, Y. Castrillejo, J. Electroanalyt. Chem. 603 (2007) 81.
[22] M.R. Bermejo, F.E. Barrado, A.M. Martinez, Y. Castrillejo, J. Electroanalyt. Chem. 617 (2008) 85.
[23] C. Caravaca, G. De Cordoba, M.J. Tomas, M. Rosada, J. Nucl. Mater. 360 (2007) 25.
[24] S.A. Kuznetsov, M. Gaune-Escard, J. Electroanalyt. Chem. 595 (2006) 11.
[25] S.A. Kuznetsov, L. Rycerz, M. Gaune-Escard, J. New. Mater. Electrochem. Systems 9 (2006) 313.
[26] S.A. Kuznetsov, M. Gaune-Escard, in: Proceedings of the Seventh International Symposium on Molten Salts Chemistry and Technology, Toulouse, France, vol. 2, 2005, p. 855.
[27] R.S. Nicholson, I. Shain, Anal. Chem. 36 (1964) 706.
[28] H. Matsuda, Y. Ayabe, Z. Elektrochem. 59 (1955) 494.
[29] M.V. Smirnov, Electrode Potentials in Molten Chlorides, Nauka, Moscow, 1973.
[30] K.E. Johnson, J.R. Mackenzie, J. Electrochem. Soc. 116 (1969) 1697.
[31] G.N. Papatheodorou, O.J. Kleppa, J. Phys. Chem. 78 (1974) 176.
[32] Z. Galus, Fundamentals of Electrochemical Analysis, Ellis Horwood, London, 1994.
[33] P. Delahay, New Instrumental Methods in Electrochemistry: Theory, Instrumentation and Application to Analytical and Physical Chemistry, Interscience, New York, 1954.
[34] R.S. Nicholson, Anal. Chem. 37 (1965) 1351.
[35] S.A. Kuznetsov, S.V. Kuznetsova, P.T. Stangrit, Soviet Electrochem. 26 (1990) 55.
[36] S.A. Kuznetsov, H. Hayashi, K. Minato, M. Gaune-Escard, Electrochim. Acta 51 (2006) 2463.
[37] J.R. Macdonald, Impedance Spectroscopy, Wiley, New York, 1987.